ELSEVIER

Marine Geology 160 (1999) 327–337

MARINE GEOLOGY
INTERNATIONAL JOURNAL OF MARINE GEOLOGY, GEOCHEMISTRY AND GEOPHYSICS

www.elsevier.nl/locate/margeo

Design and application of a new free fall in situ resistivity probe for marine deep water sediments

A. Rosenberger [a,*], P. Weidelt [b], C. Spindeldreher [a], B. Heesemann [a], H. Villinger [a]

[a] *University of Bremen, FB5, Postfach 330440, 28334 Bremen 33, Germany*
[b] *Inst. f. Geophysik and Meteorologie, TU-Brunswick, Germany*

Received 15 May 1998; accepted 12 February 1999

Abstract

We have developed a new type of sediment penetrating in situ probe which logs electrical resistivity in marine and limnic sediments in the uppermost 3.5 m. As the instrument is fitted to a Lister-type heat-flow instrument, combined thermal and electrical conductivity measurements are possible. The probe incorporates no moving mechanical parts, is built to operate in water-depths up to 4000 m and is relatively easy to deploy. Two separate electrode arrays provide for an instant repeatability test and rapid data quality assessment. The probe was extensively tested in the laboratory. Field tests in Lake Konstanz and in the North Sea produced consistent results. This paper gives a description of the design of the probe and the test results. A theoretical derivation of the probe's configuration factor is presented and theoretical results are verified in laboratory tests.
© 1999 Elsevier Science B.V. All rights reserved.

Keywords: marine sediments; electrical resistivity; in situ testing; circular Wenner array; configuration factor

1. Introduction

The electrical properties of unconsolidated sediments are generally linked to other physical properties through a series of empirical relationships. Based on the investigations of Archie (1942) numerous authors have published results linking electrical resistivity to sediment porosity and density. The majority of these papers concentrate on sedimentary rocks with low to medium porosities whereas investigations on high porosity unconsolidated sediments are still rare. Descriptions of experimental results, linking electrical resistivity of unconsolidated sediments to porosity can be found in Jackson (1975), Cheesmann et al. (1991), Cheesmann et al. (1993) and Kermabon et al. (1969). While those studies focus on a marine environment, a similar application was developed by Campanella and Weemes (1990) for geotechnical investigations onshore where the instrument is combined with a piezo-cone penetrometer. Offshore applications of cone penetrometer testing (CPT) are described in Lunne et al. (1997) where combined CPT and electrical resistivity measurements are discussed as well.

* Corresponding author. Fax: +49-421-218-7163; E-mail: andreas@geophys2.uni-bremen.de

0025-3227/99/$ - see front matter © 1999 Elsevier Science B.V. All rights reserved.
PII: S0025-3227(99)00023-7

Instruments for marine applications basically fall in the two categories of penetrating and non-penetrating probes. While measurements on the seafloor with non-penetrating techniques have the inherent advantage that they do not disturb the sediment structure in the measuring process, they require that an inversion scheme is applied to the data to yield resistivity vs. depth. Penetrating instruments on the other hand may cause some disturbance, but deliver direct resistivity–depth logs with high vertical resolution.

Jackson (1975) uses a pad fitted with focusing electrodes which is lowered on to the sediment surface. In this way an average resistivity from a zone within 0.5 m of the sediment water interface can be measured. The instrument of Cheesmann et al. (1991, 1993) is also of the non-penetrating variety. His system consists of an electromagnetic transmitter and one or more receivers which are towed close to the seafloor. Traveltimes of the electromagnetic pulse are directly related to seafloor resistivities and the data of a multi-receiver system can be inverted (Cheesmann et al., 1987) for a two dimensional resistivity–depth profile.

The initial instrument of Kermabon et al. (1969) most closely resembles the operating principle of our probe. A lance-like shaft with a weight on top is free-fall deployed into the sediment. The shaft carries a four-point vertical electrode array at its tip which is extended to push against the sediments during controlled extraction of the instrument thus providing a resistivity vs. depth log.

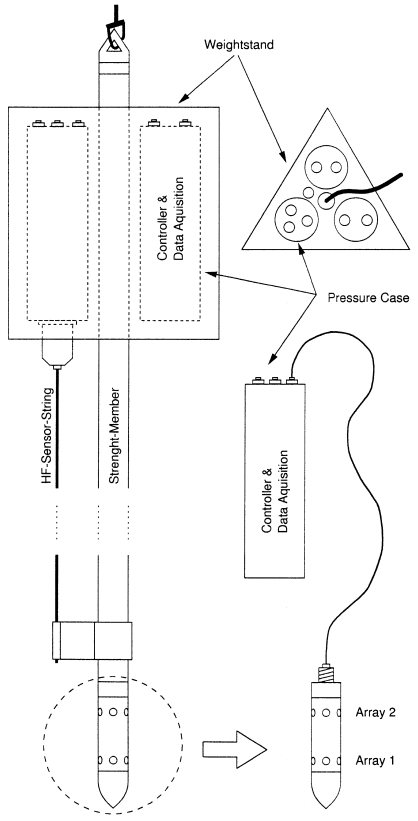

Fig. 1. The resistivity tip (circled) is part of a Lister type heat-probe. The backbone of the assembly is the so-called strength member which carries a 500 kg weight stand of triangular shape on top. The electronics are built into pressure cases which fit into holes in the weight stand.

2. Description of our instrument

A basic sketch of our instrument platform is given in Fig. 1. The assembly is actually a Lister-type (violin-bow) heat-probe (Hyndman et al., 1979) comprising a 500 kg weight-stand which also houses the pressure cases of the data-loggers. A rod carries the electrode arrays at the tip and also serves as a strength member for the thermistor sensor string.

The tip carrying the electrodes is shown in more detail in Fig. 2. Two identical horizontal circular electrode arrays with a pair of opposing current electrodes and four potential electrodes equally spaced between them are mounted in an electrically insulating highly abrasion resistant plastic material (PVDF). The electrodes are made of sea-water grade bronze.

Each of the electrodes is wired to a deep sea connector on top of the probe, from where a cable is running through the hollow strength member to the pressure case which houses the electronics of the controller and data-logger. After assembly of the wiring, the interior void of the tip is taken up by a PVC-body, the remaining volume is filled with a non-conducting mineral oil.

The mechanical design is directed to make the probe resistant to the high ambient pressure in deep-sea experiments and was successfully tested in a pressure chamber for a simulated water-depth of 4000 m.

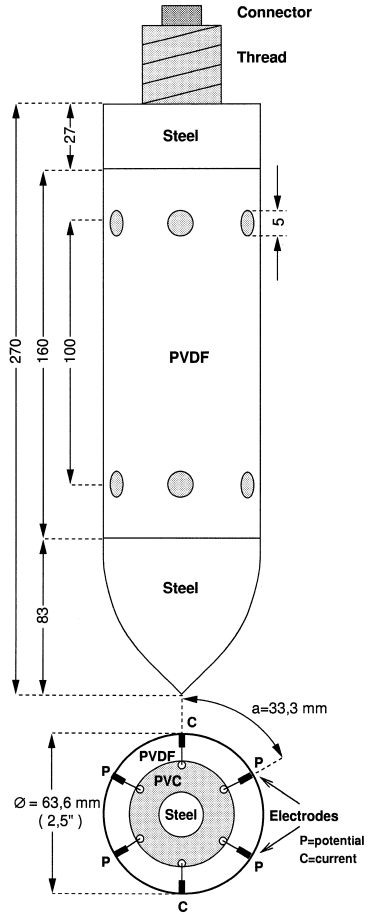

Fig. 2. An enlarged view of the resistivity tip. The skeleton is made of stainless steel, the electrodes sit in a non-conducting plastic material. The interior void is taken up by another plastic body and the small remaining volume is filled with mineral oil. In this way the tip can withstand ambient pressure equivalent to 4000 m water-depth.

2.1. Measuring principle

The two circular electrode arrays (Fig. 2) are operated independently. A DC constant current source delivering 10 mA (up to a maximum potential difference of 30 V) is reversed with a frequency of 1200 Hz to provide a 600 Hz alternating rectangular-waveform current. One complete cycle is fed to the current electrodes of the first array and 10 samples of the resulting potential are taken synchronously from the corresponding potential electrodes which are wired in parallel within each array. The first array is then disconnected and the next cycle is fed to the second array where the sampling process repeats.

The 10 samples from one individual array are finally combined into one single RMS value. Thus, both arrays are measured in a time-multiplex fashion with final sampling frequencies of 300 Hz. Additionally the datalogger samples an acceleration sensor and a pressure sensor which are both located in the pressure case. Those samples are taken whenever the arrays are switched so that acceleration and pressure is sampled with a frequency of 300 Hz as well.

Block schematics and a simple timing diagram are presented in Fig. 3. The central controlling unit for the timing is a Motorola 68332 micro-controller with an internal time processing unit (TPU) which also controls data acquisition and storage on to a 3.5″ hard disk with 500 MB capacity.

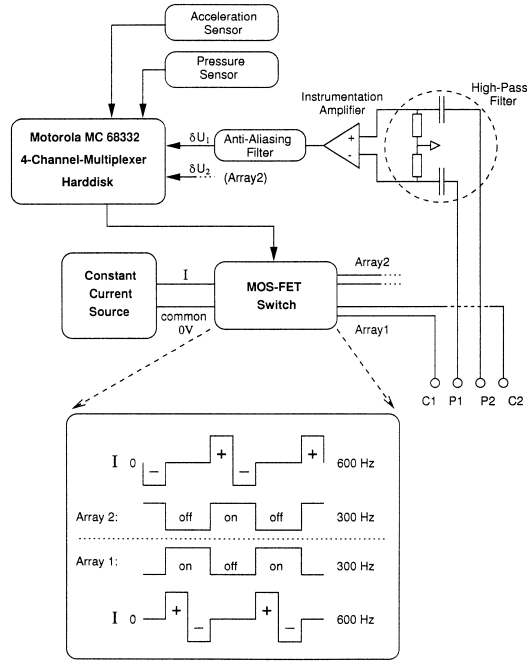

Fig. 3. The block diagram of the electronics. A Motorola MC-68332 micro-controller manages timing and data acquisition on a small hard-disk. The constant current source is transformed into a square wave-form which in turn is fed to either one of the arrays. A simple timing diagram is shown at the bottom. Ten samples are synchronously taken from the potential electrodes of the active array and an RMS value is calculated. While arrays are interchanged the pressure and acceleration sensors are sampled.

While geotechnical instruments for resistivity logging like that of Campanella and Weemes (1990) use four annular (or ring) electrodes in a vertical array on a cylindrical body we employed circular arrays of (ideally point-) electrodes in our configuration.

The reasoning behind that was guided by the fact that we have little or no control over the penetration process as the probe is lowered into the sediment on a wire of several thousand meters of length. Previous experiments measuring acceleration of a gravity corer during penetration suggest that initial penetration speeds can vary between ± 1 m/s and the penetration can be rather erratic due to ship's heave and cable eigenmodes. Employing two vertically separated arrays offers the possibility of an in-built repeatability test. During a 'clean' penetration, data from the upper array should closely resemble the data from the lower array just with a time delay proportional to the velocity of the probe relative to the sediments. Erratic movement, tilting after penetration and dynamic effects of a boundary-layer are easy to identify in a first visual inspection of the data.

To accommodate two independent arrays under the constraints of the Lister-probe design, we choose to implement the vertical circular arrays. In order to verify that the physical dimensions of our probe are adequate, we compare the configuration factor as predicted by theory with the results from experimental calibration in Section 3.

3. Configuration factor of a circular Wenner-type array on a cylindrical probe

The four-ring electrode array on a non-conducting cylindrical body in a conducting environment has been investigated theoretically by Won (1987) and Ridd (1994), whereas the problem of a circular point-electrode array on a *conducting* cylinder of finite length in a *non-conducting* environment has been considered by Weidelt and Weller (1997). The corresponding problem of finding the configuration factor of a circular point-electrode array on a *non-conducting* cylinder of infinite length in an unbounded *conducting* space is treated in Section 3.1, where we also verify the theoretical results for our 'non-ideal' probe in laboratory experiments.

3.1. Theoretical derivation of the configuration factor

Assuming cylindrical coordinates, point of observation $\mathbf{r}$ and source point $\mathbf{r}_0$ are given by:

$$\mathbf{r} = (r, \varphi, z) \text{ and } \mathbf{r}_0 = (r_0, \varphi_0, 0)$$

First we consider a uniform whole-space with resistivity ϱ. If the current I is fed at $\mathbf{r}_0$, the resulting electric pole–pole potential $V(\mathbf{r}_0|\mathbf{r})$ is:

$$V_0(\mathbf{r}_0|\mathbf{r}) = \frac{I\varrho}{4\pi R}$$

with:

$$R^2 = s^2 + z^2, \quad s^2 = r^2 + r_0^2 - 2rr_0\cos(\varphi - \varphi_0)$$

Let $r \le r_0$. Then by means of the integral representation [e.g., Watson (1966), Eq. 13.21 (10)]:

$$\frac{1}{R} = \frac{2}{\pi}\int_0^\infty K_0(\lambda s)\cos\lambda z \,\mathrm{d}\lambda$$

and the addition theorem [e.g., Watson (1966), Eq. 11.3 (8)]:

$$K_0(\lambda s) = \sum_{n=0}^{\infty} (2 - \delta_{n0})\, I_n(\lambda r)\, K_n(\lambda r_0) \times \cos n(\varphi - \varphi_0)$$

(with $\delta_{n0} = 1$ for $n = 0$ and $\delta_{n0} = 0$ for $n \neq 0$) we obtain the well-known source representation:

$$V_0(\mathbf{r}_0|\mathbf{r}) = \frac{\varrho I}{2\pi^2}\int_0^\infty \mathrm{d}\lambda \cos\lambda z \cdot \sum_{n=0}^{\infty} (2 - \delta_{n0}) \times \cos n(\varphi - \varphi_0)\, I_n(\lambda r)\, K_n(\lambda r_0) \qquad (1)$$

Here $I_n(\cdot)$ and $K_n(\cdot)$ are the modified Bessel functions of order n [e.g., Abramowitz and Stegun (1972), Chap. 9.6]. For $r \ge r_0$, the functions $I_n(\cdot)$ and $K_n(\cdot)$ are interchanged.

The cylinder of infinite length with radius a is taken into account by replacing in the whole-space potential (1), for $a \le r \le r_0$, the function $I_n(\lambda r)$ by:

$$I_n(\lambda r) + C_n(\lambda)\, K_n(\lambda r)$$

Then $C_n(\lambda)$ is determined from the boundary condition:

$$\left.\frac{\partial V}{\partial r}\right|_{r = a^+} = 0$$

yielding:

$$C_n(\lambda) = -\frac{I_n'(\lambda a)}{K_n'(\lambda a)}$$

For $r = r_0 = a$, considerable simplification achieved by using the Wronskian:

$$K_n'(x)\,I_n(x) - I_n'(x)\,K_n(x) = -\frac{1}{x}$$

with $x := \lambda a$. Then:

$$V(\mathbf{r}_0|\mathbf{r}) = \frac{\varrho I}{2\pi^2 a}\int_0^\infty \mathrm{d}x \cos(xz/a) \sum_{n=0}^{\infty} (2-\delta_{n0}) \times \cos n(\varphi-\varphi_0)\, f_n(x) \quad (2)$$

with:

$$f_n(x) := -\frac{K_n(x)}{xK_n'(x)} > 0$$

The potential of a ring electrode, as given by Ridd (1994), corresponds to the term $n = 0$.

The potential V_W of an azimuthal Wenner array at $z = 0$ is obtained from the superposition of four pole–pole potentials. With the notation of Fig. 4 we have:

$$V_W = V(\mathbf{r}_A|\mathbf{r}_M) - V(\mathbf{r}_A|\mathbf{r}_N) - V(\mathbf{r}_B|\mathbf{r}_M) + V(\mathbf{r}_B|\mathbf{r}_N) \quad (3)$$

Hence, V_W depends on the sum:

$$\cos(n\varphi_{AM}) - \cos(n\varphi_{AN}) - \cos(n\varphi_{BM}) + \cos(n\varphi_{BN}) = 2\left(\cos\frac{n\pi}{3} - \cos\frac{2n\pi}{3}\right) = 4\sin\frac{n\pi}{2}\sin\frac{n\pi}{6} = \begin{cases} 0, & n \text{ even} \\ 2, & n = 6m+1 \\ -4, & n = 6m+3 \\ 2, & n = 6m+5 \end{cases} \quad (4)$$

with $m = 0,1,2,\ldots$

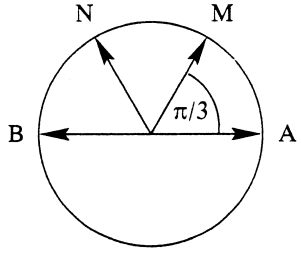

Fig. 4. Illustration of the indices used in the theoretical derivation of the configuration factor of our probe.

The configuration factor k is defined by:

$$\varrho = k\frac{V_W}{I} \quad (5)$$

Therefore Eqs. (2)–(5) yield as integral representation of a/k:

$$\frac{a}{k} = \frac{2}{\pi^2}\int_0^\infty \mathrm{d}x \sum_{m=0}^{\infty} \left[f_{6m+1}(x) - 2f_{6m+3}(x) + f_{6m+5}(x)\right] \quad (6)$$

Let us briefly investigate the convergence of the sum in Eq. (6). From Eqs. 9.7.8 and 9.7.10 of Abramowitz and Stegun (1972) it is inferred that for $n \gg x$ the function $f_n(x)$ is approximated by:

$$f_n(x) \simeq \frac{1}{\sqrt{n^2+x^2}}$$

which yields for $m \gg \max(x,1)$ the asymptotic expansion:

$$f_{6m+1}(x) - 2f_{6m+3}(x) + f_{6m+5}(x) = \frac{1}{27m^3} - \frac{1}{18m^4} + \frac{58-3x^2}{972m^5} + \mathscr{O}\left(\frac{1}{m^6}\right)$$

With this result, the convergence of the infinite sum is easily controlled.

As a function of x, the integrand decays monotonically such that the upper limit of integration at $x = 12$ yields already a six digit accuracy. Numerical evaluation of the right-hand side of Eq. (6) gives 0.099968 implying:

$k = 10.00319 \cdot a$

The radius of our probe is $a = 0.0318$ m. Therefore the configuration factor should be:

$k_{\mathrm{Probe}} = 0.3181\,\mathrm{m}$

3.2. Experimental results

The real resistivity probe deviates from the ideal one under consideration in the Section 3.1 mainly in two properties:

- The cylinder is of *finite* length, i.e., the array dimensions (the cylinder diameter and the distance of the arrays from the end of the non-conducting electrode carrier) are commensurate.
- The electrodes have, in contrast to ideal 'point-electrodes', a finite size.

To verify that theory still properly describes our instrument, we have calibrated each individual array of three different probe tips of identical design in salt-water of known resistivity.

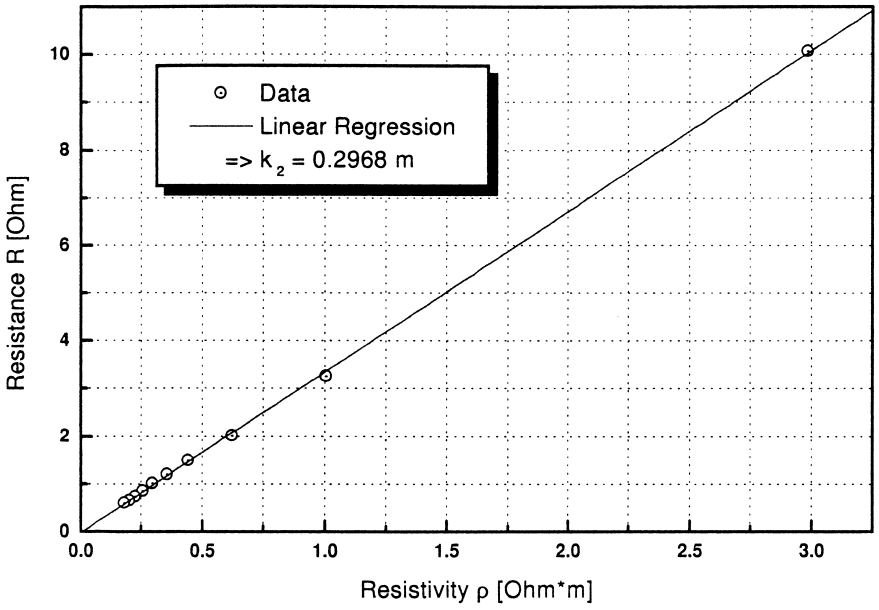

Fig. 5. Example from the experimental determination of the configuration factor for one of the arrays out of six on three different probe tips. Measurements of resistivity were taken with a calibrated instrument in salt-water of different NaCl concentrations. The values are plotted vs. resistance as measured on the probe-tip array. Linear regression yields a configuration factor of $k = 0.2968$ m for this particular array.

A plastic drum 0.8 m high with a diameter of about 1 m was filled with salt-water and for each experiment the NaCl concentration was varied. A commercially available instrument was used to measure the resistivity of the solution and resistance was measured with one of the arrays of the probe.

An example of the result for one individual array is given in Fig. 5. The average configuration factor of six independent experiments for the six individual arrays turns out to be $\bar{k} = 0.2969$ m with a standard deviation of ± 0.0051 m which is in good agreement with theoretical results, considering the deviation from ideal assumptions, and verifies at the same time that the physical dimensions, i.e., the distance of the electrode arrays from metal parts of the probe, were chosen reasonably well.

4. Operation and field tests

For practical field work the operating procedures were designed along the requirements for heat-flow measurements. Although the instrument works completely independent from the heat-probe, joint resistivity and heat-flow measurements will be the general mode of operation for our purposes.

Data acquisition and control electronics as well as the batteries are built into one pressure case which also carries a pressure sensor. The acquisition program is initialised by pre-setting pressure thresholds at which the probe starts or stops data acquisition. As soon as the probe starts to sample the electrode arrays, it also reads and stores values from the acceleration sensor. In a deep-sea experiment this enables operations in ‘pogo’ style (Hyndman et al., 1979). In water-depth of several thousand meters the probe is lowered to the bottom once and is lifted out of the seafloor sediments only for a couple of hundred meters after a penetration. In the meantime the ship moves on to the next station where the probe is lowered into the sediments again. In this way a number of experiments along a profile can be conducted without bringing the instrument back on board.

If pressure thresholds are set appropriately, the resistivity probe will not acquire data when the ship

moves on to another site and power consumption and data-storage requirements are minimised. In the current configuration the resistivity probe will operate continuously for about 6 h. This limit is imposed by battery and not by data-storage capacity.

Two field tests were conducted in early springtime 1997 on Lake Konstanz, Southern Germany and in early summer of the same year in the North Sea at 54°03′N, 8°00′E.

In the Lake Konstanz experiment the instrument was deployed from a barge several times into the soft, clayey sediments off the Swiss shore in a water-depth of about 80 m. As the barge was not anchored it was drifting during operations. While it was thus possible to lower the instrument into the sediment without any significant tilt, the extraction process always tilted the instrument considerably. The same is true for the North Sea experiment in waters of about 30 m depth using the German research vessel ALKOR.

Since our acceleration sensor is tilt sensitive, data from the extraction cannot be mapped from a time to a depth scale by means of double integration of the acceleration data.

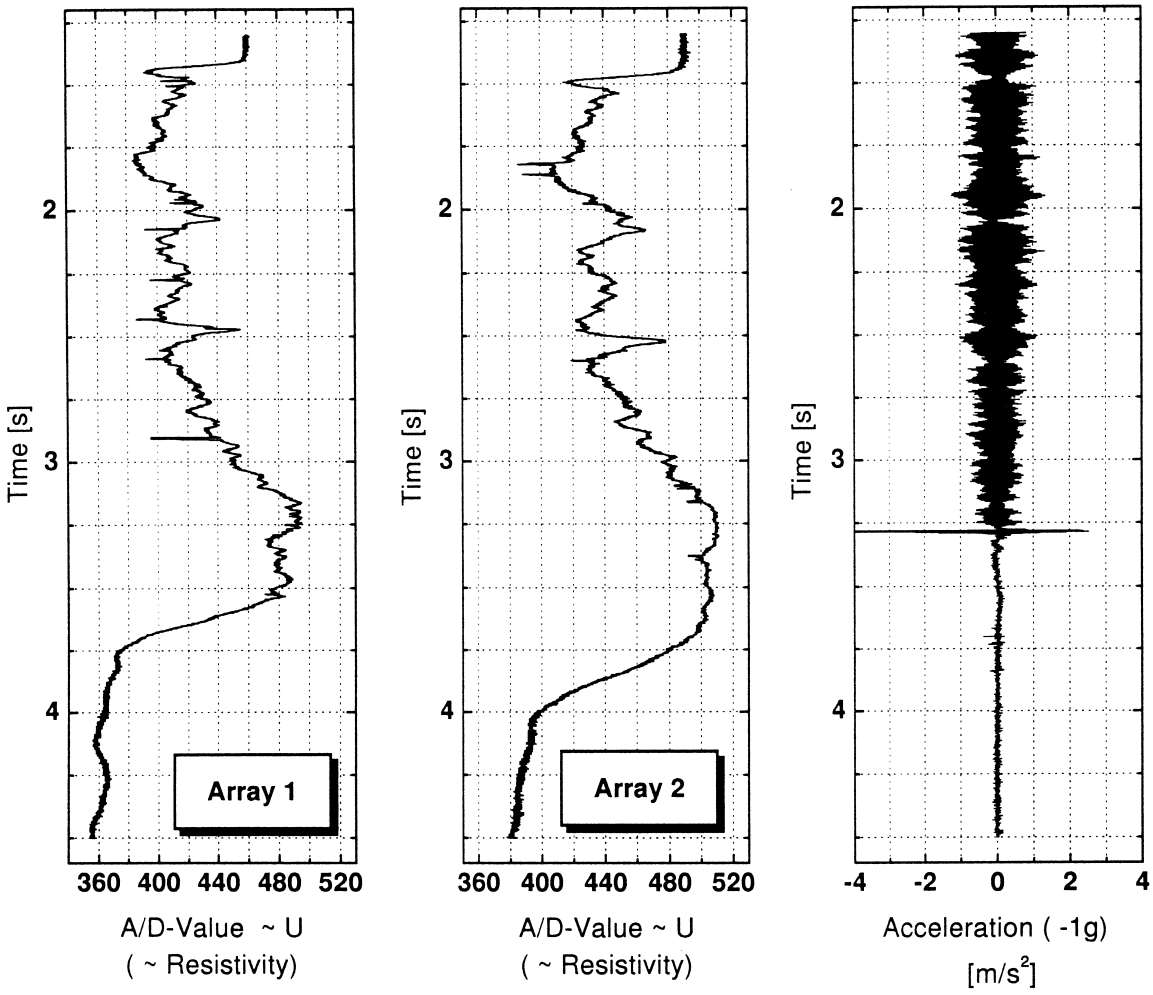

Fig. 6. Data from the Lake Konstanz field test. The left two panels show data from the lower *array 1* and the upper *array 2*, respectively in units of A/D converter values over time. The right panel shows acceleration in units of m/s^2 where $1g$ has already been subtracted. Down to about 3.2 s, before the weight stand settles to the bottom (large amplitude), the signal is dominated by cable-strum.

5. Field data

Fig. 6 shows the raw data from the Lake Konstanz test. In the first two panels the *uncalibrated* values from the A/D converter of each of the two arrays are plotted vs. the time scale. The *lower* array (array 1) enters the sediments at 1.4 s.

It can clearly be seen that those are data from a penetration as the values from the *lower* array lead in time against the data from the *upper* array (array 2). The data from the *lower* array also show more detail which is probably due to the fact that the sediment is less disturbed close to the penetrating tip than it is at the location of the *upper* array.

The right panel shows data from the acceleration sensor where the background value for $1g$ was already subtracted. Even when the lance has already entered the sediments, acceleration values are obscured by cable strum. The most prominent feature in the acceleration data is the large event when the weight stand of the probe settles on the lake bottom.

The first panel on the left in Fig. 7 shows velocity of the probe vs. time. Those data were computed from acceleration by backward integration starting at

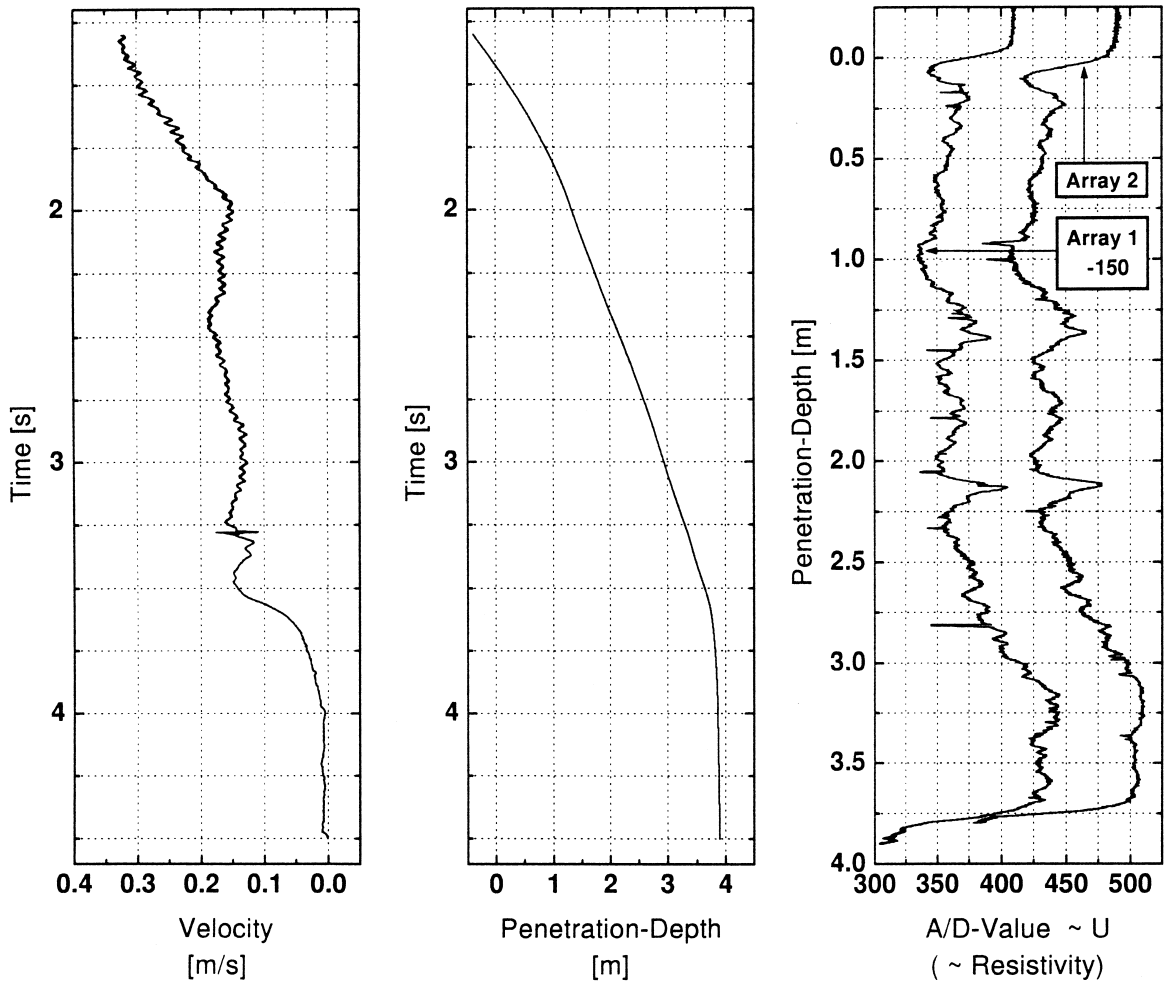

Fig. 7. Data from the Lake Konstanz field test. Velocity and penetration depth vs. time data are derived from acceleration by integration. The penetration depth vs. time curve is used to map the data from the resistivity arrays onto a depth scale. Data from both array now agree very well in depth and amplitude. Here the data from *array 1* are offset by 150 units for easier display.

a time where the probe is at rest, using $v(t_{\text{final}}) = 0$ m/s as an integration constant. After the weight stand has settled on the bottom it still takes about 0.7 s for the probe to be completely at rest.

The middle panel Fig. 7 shows the result of the second integration over velocity. Here integration can either be carried out in a time-forward direction, setting z at the time of penetration as seen in the resistivity data $z(t_{\text{pen}}) = 0$ m or, like in this case, integration can be carried out backward, again taking the time when the weight stand settles as the time associated with the maximum penetration. This value in turn is given by the distance of the *lower* array from the weight stand bottom yielding $z(t_{\text{final}}) = 3.8$ m as an integration constant.

The time–depth relationship can now be used to map the uncalibrated resistivity data onto a depth scale applying a constant shift of 0.1 m to the data from *lower* array which corresponds to the array separation. The result is shown in the panel on the right in Fig. 7 with the data values offset for easier display. Data from both arrays now agree very well,

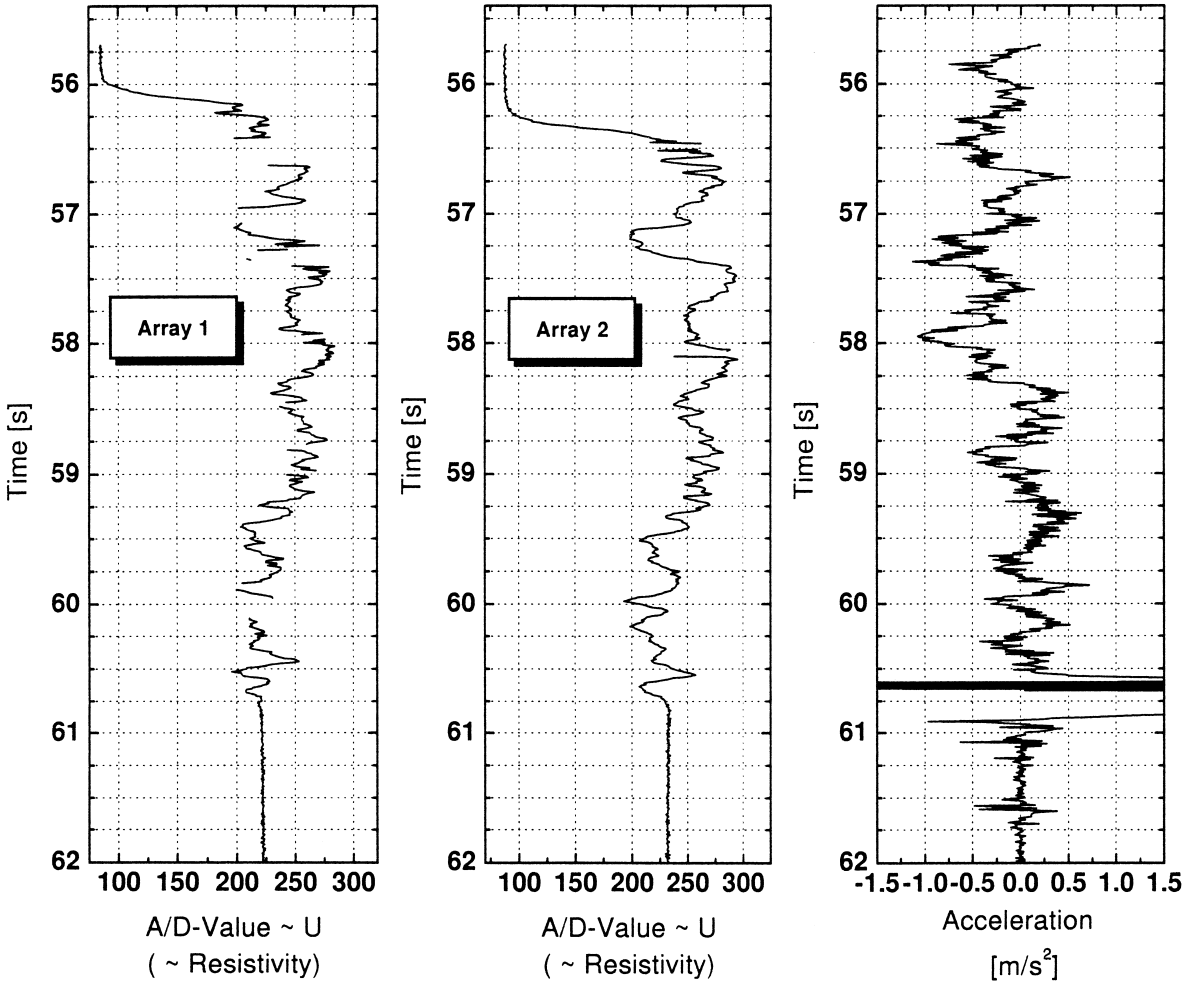

Fig. 8. Data from the North Sea field test. The left two panels show data from the lower *array 1* and the upper *array 2*, respectively in units of A/D converter values over time. *Array 1* shows missing data probably when it passed strands of shell fragments in the sediment which forced the amplifier into saturation. The upper *array 2* is much less affected because the sediments are disturbed to a greater extent already. The right panel shows acceleration of the probe during penetration. The high amplitudes at about 60.5 s mark the time when the weight stand hits the bottom.

with an accuracy in depth generally better than 3 cm. Formation factors may now be calculated by normalising the data with an average value of the data taken in the water-column close to the lake bottom.

Figs. 8 and 9 sketch the same sequence of curves for the North Sea experiment. Raw data of uncalibrated resistivity and acceleration are shown in the left two panels and in the right panel of Fig. 8, respectively. The sediments at this particular location are of pelagic type with embedded strands of shell fragments. The signal from the *lower* array exceeded the dynamic range of the pre-amplifier passing those shell-fragment layers with the result that some data are missing. However, the second array travelling through an already '*smoothed*' sediment column is less affected from those thin layers.

In Fig. 9 the velocity and depth vs. time curves for the North Sea experiment are given. The rightmost panel shows the uncalibrated resistivity data mapped to a depth scale. Again correlation of the data from both arrays is excellent in amplitude as well as in depth. The formation factor in this case would vary in the sediment column between 2.2 and 3.3 which in turn would yield porosities according to

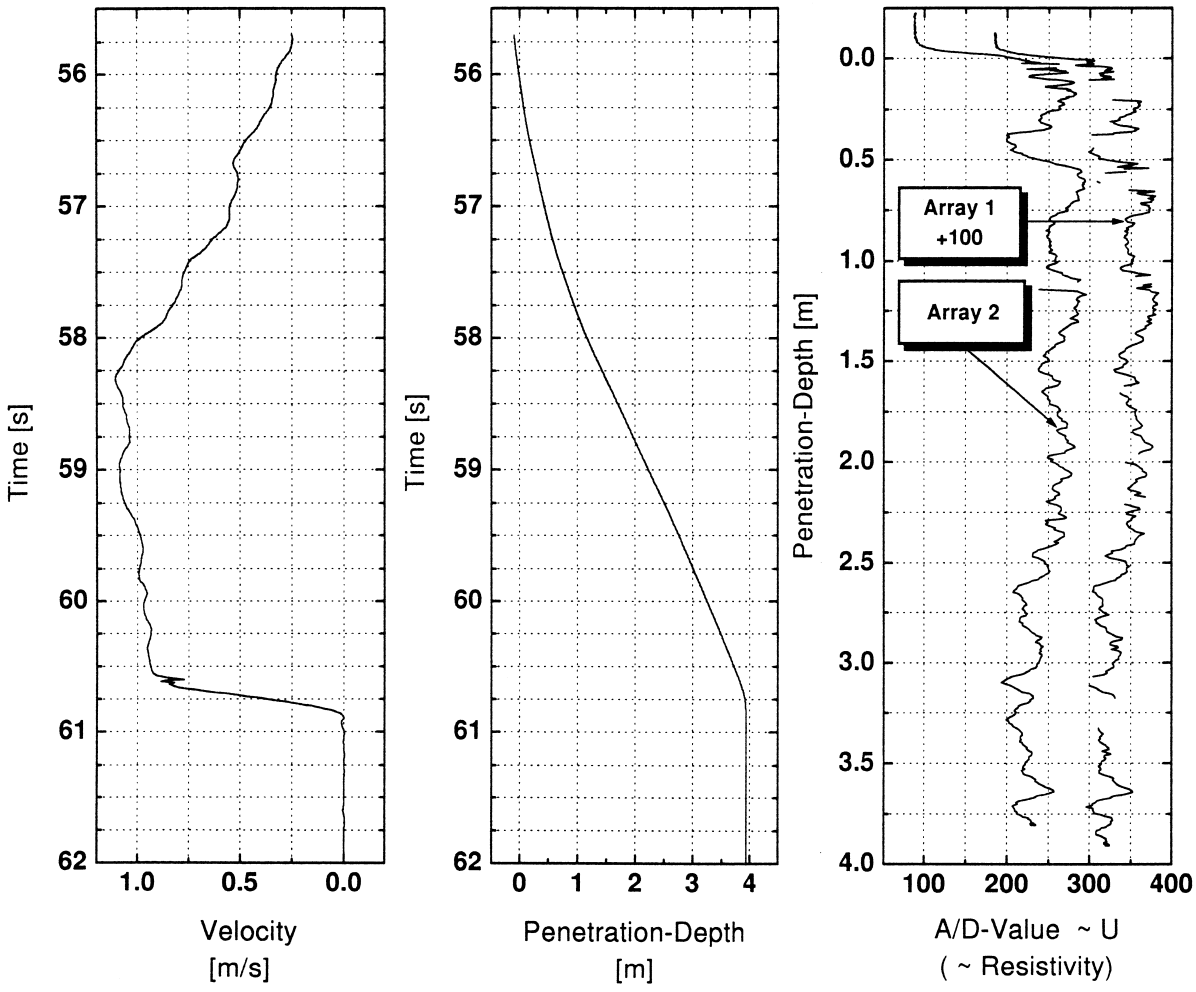

Fig. 9. Data from the North Sea field test. Velocity and penetration depth vs. time data are derived from acceleration by integration. The penetration depth vs. time curve is used to map the data from the resistivity arrays onto a depth scale. Data from both array now agree very well in depth and amplitude. Here the data from *array 1* are offset by 100 units for easier display.

Archie's law (Archie, 1942) between 54% and 67%, using $m = 2$ for the cementation factor. Those values are very reasonable for the pelagic type sediments at that particular location.

6. Conclusions

It has been shown that a relatively simple instrument which is inserted into marine sediments in an uncontrolled fashion can provide useful resistivity logs which in turn may be used to derive related physical properties of the sediment. The two independent circular arrays with vertical separation introduce a possibility to assess data quality and have served us as well to gain confidence in our instrument through a built-in repeatability test. Data from a simple acceleration sensor can be taken to map data from time domain to a depth scale. However, since our acceleration sensor is sensitive to tilt as well this is true only when the instrument penetrates the sediment with negligible tilt. This should not pose a problem in the deep sea but can be particularly difficult to achieve operating from a ship in shallow waters. Optimally one would use a system which would measure tilt and depth vs. time directly rather than compute the solution via two-fold integration.

Acknowledgements

We thank the people of Wolfgang Fulda and Andre Bruenkers here at the University of Bremen, who designed and engineered the probe-tip mainly in their free time. We also thank the journal referees.

References

Abramowitz, M., Stegun, I.A., 1972. Handbook of Mathematical Functions, 2nd edn. Dover, New York.

Archie, G.E., 1942. The electrical resistivity log as an aid in determining some reservoir characteristics. Transactions of the American Institute of Mining and Metallurgical Engineers 147, 54–62.

Campanella, R.G., Weemes, I., 1990. Development and use of an electrical resistivity cone for groundwater contamination studies. Canadian Geotechnical Journal 27, 557–567.

Cheesmann, S.J., Edwards, R.N., Chave, A.D., 1987. On the theory of sea-floor conductivity mapping using transient electromagnetic systems. Geophysics 52, 204–217.

Cheesmann, S.J., Law, L.K., Edwards, R.N., 1991. Porosity determination of sediments in Knight Inlet using a transient electromagnetic system. Geomarine Letters 11, 84–89.

Cheesmann, S.J., Law, L.K., Louis, B.S., 1993. A porosity mapping survey in Hecate Strait using a seafloor electro-magnetic profiling system. Marine Geology 110, 245–256.

Hyndman, R.D., Davis, E.E., Wright, J.A., 1979. The measurement of marine geothermal heat flow by a multipenetration probe with digital acoustic telemetry and in situ thermal conductivity. Marine Geophysical Research 4, 181–205.

Jackson, P.D., 1975. An electrical resistivity method for evaluating the in-situ porosity of clean marine sands. Marine Geotechnology 1, 91–115.

Kermabon, A., Gehin, C., Blavier, P., 1969. A deep-sea electrical resistivity probe for measuring porosity and density of unconsolidated sediments. Geophysics 34, 554–571.

Lunne, T., Robertson, P.K., Powell, J.J.M., 1997. Cone Penetration Testing, 1st edn. Blackie Academic and Professional, London, UK.

Ridd, P.V., 1994. Electrical potential due to a ring electrode. IEEE Journal of Oceanic Engineering OE 19, 464–467.

Watson, G.N., 1966. A Treatise on the theory of Bessel Functions, 2nd edn. Cambridge Univ. Press, Cambridge, UK.

Weidelt, P., Weller, A., 1997. Computation of geoelectrical configuration factors for cylindrical core samples. Scientific Drilling 6, 27–34.

Won, I.J., 1987. The geometrical factor of a marine resistivity probe with four ring electrodes. IEEE Journal of Oceanic Engineering OE 12, 301–303.